Fusion Engineering and Design 185 (2022) 113320

Contents lists available at ScienceDirect

Fusion Engineering and Design

journal homepage: www.elsevier.com/locate/fusengdes

Experimental and numerical evaluation of the neutral beam deposition profile in KSTAR

B. Na [a,*], J. Kang [a], M.W. Lee [b], L. Jung [a], S.H. Hahn [a], J.W. Yoo [a], J.H. Jeong [a], J. Ko [a], C. Sung [b]

[a] Korea Institute of Fusion Energy (KFE), Daejeon, Republic of Korea
[b] Korea Advanced Institute of Science and Technology, Daejeon, Republic of Korea

ARTICLE INFO

Keywords:
Magnetic fusion
Tokamak
KSTAR
Neutral beam current drive

ABSTRACT

In this article the neutral beam deposition profile of each neutral beam source in KSTAR is reported. Since the neutral beam system of KSTAR is the main heating and current drive source, it is crucial to estimate and reconstruct the neutral beam deposition profile with high accuracy. A fully non-inductive discharge experiment is conducted to minimize Ohmic current effect on the interpretation. An each beam source is switched off one by one longer than the current diffusion time scale. Reconstructed beam driven current is derived by extracting the total current profile from non-beam driven current components such as bootstrap, electron cyclotron, and Ohmic. By comparing numerical beam modeling, beam driven deposition profile per each beam source is quantitatively interpreted.

1. Introduction

One of the main milestones of KSTAR [1] is to demonstrate a long-pulse operation with fully non-inductive condition. In order to sustain plasma current, neutral beam current drive (NBCD) [2–4] system is installed as the main heating and current (H&CD) system. The NBCD profile is crucial in terms of designing the steady state operation scenario. Experimental investigation and verification of NBCD had been widely conducted in International Tokamak physics activity joint experiments [5], NSTX [6], and DIII-D [7,8]. However, the actual NBCD profile in KSTAR has never been explored systematically. Thus, the first systematic approach to deriving a neutral beam deposition profile in KSTAR is performed after operation of the second neutral beam injection (NBI) system. To investigate NBI characteristics, this paper reports the dedicated experiment and numerical modeling activity to evaluate neutral beam deposition profile. The remainder of the paper is organized as follows. Section 2 presents experiment purpose and setup of a low loop voltage discharge. In Section 3, reconstructed and computed NBCD profile are compared. Finally, conclusions are presented and future plans are discussed in Section 4.

2. Experiment setup

2.1. A fully non-inductive discharge

In order to analyze neutral beam deposition profile, it is required to subtract neutral beam current drive profile from total current profile. To minimize external heating sources, a low loop voltage and high beam driven current fraction scenario is prepared. The experimental setup for this experiment is designed to draw high efficiency of the NB current drive (NBCD) in the known way that is called as 'high β_p' discharges [9].

As shown in the figure 3 of Ref. [10], near-center electron cyclotron current drive (ECCD) injections (mirror aim target vertical target Z < +10 cm from the midplane) onto diverted H-mode at high-B_T invoke a stationary high β_p shot with fully non-inductive current drive. Under this experiment, R_{major} = 1.8 m, $B_{T,axis}$ = 2.49 T, I_p ~ 450–500 kA, are used to develop a diverted high-β_p discharge, P_{NB} ~ 5 MW with 4 NB sources 90(NBI1-A)/90(NBI1-B)/70(NBI1-C)/60(NBI2-B) keV, κ ~1.9, q_{95} ~ 8.8, β_p ~ 2.2-2.4, l_i ~ 0.8, β_N ~ 1.6-2.0, as shown in Fig. 1.

The fully non-inductive condition obtained in the shot number 27281, as shown in Fig. 1, can be found by scanning the appropriate I_p level under the same heating conditions that achieve the reference loop voltage signal to be very close to zero, where it is assumed that the Ohmic current drive vanishes; the reference loop voltage signal was chosen as the unintegrated voltage reading of the flux loop diagnostics at the midplane inboard. The I_p scan clarified the total amount of the noninductive current drive is about 480 kA, which was chosen as the I_p target for the discharge in Fig. 1.

As mentioned above, the gyrotron aiming is important for the onset of the fully noninductive CDs ; Among the two gyrotrons used in the discharge, only the EC4 140 GHz gyrotron has been used to trigger the

* Corresponding author.
E-mail address: bna81@kfe.re.kr (B. Na).

https://doi.org/10.1016/j.fusengdes.2022.113320
Received 7 July 2022; Received in revised form 27 September 2022; Accepted 10 October 2022
Available online 15 November 2022

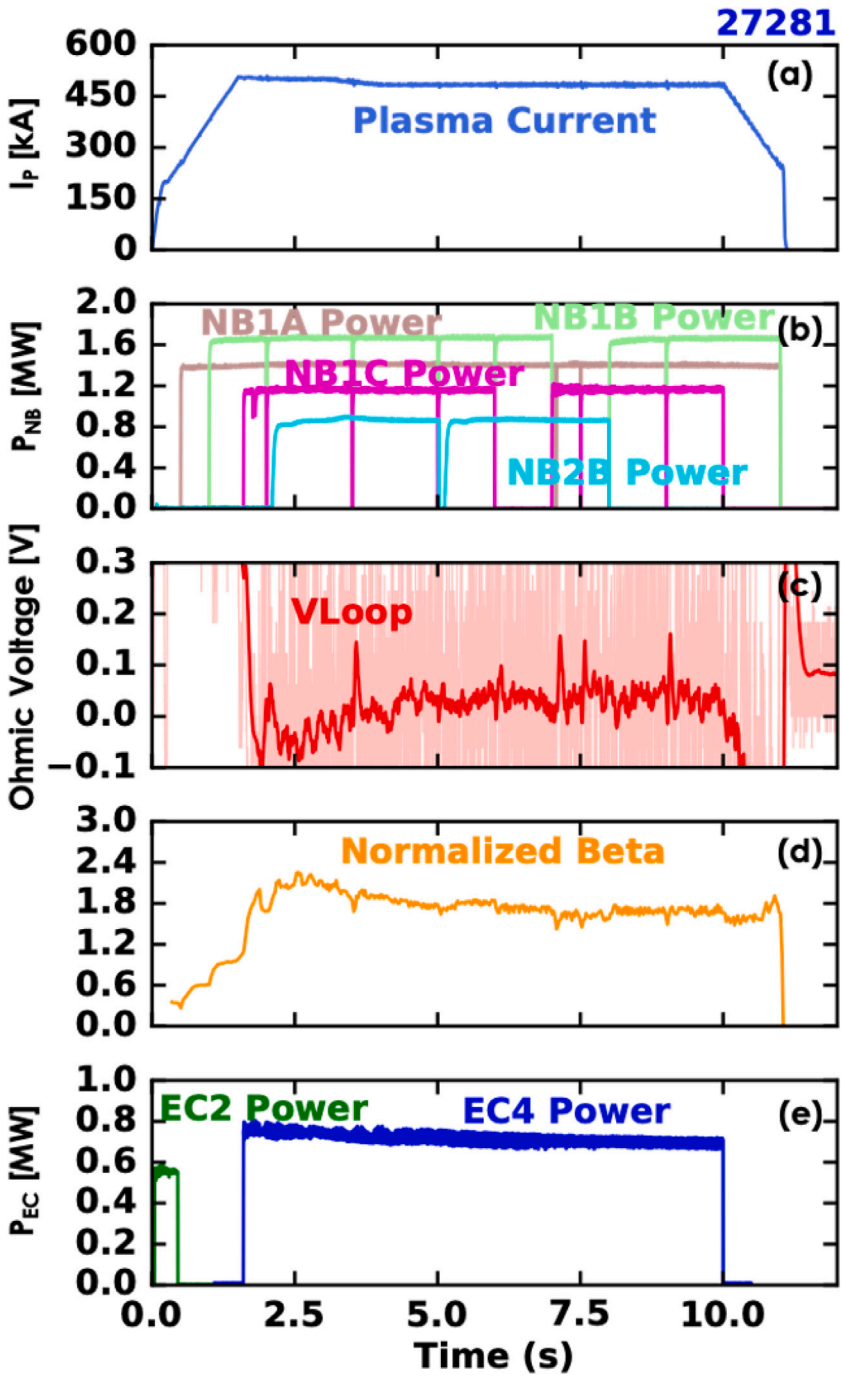

Fig. 1. Shot 27281 with fully non-inductive discharge. From top to bottom, (a) plasma current [kA] (b) beam power in MW by source (c) loop voltage PCLV23 measured at the reference flux point (both raw data and averaged data shown) (d) Normalized β_N and (e) gyrotron injection profiles. NBI1-A/B/C and NBI2-B denote the ion source names shown in Fig. 2. Two gyrotrons, labeled as EC2 and EC4 respectively, are used, but only the EC4 has been used at the center of plasma in order to onset the high β_p condition.

high-β_p. Targeting the beam toroidal angle = 15 degrees and vertical Z position = 2.7 cm at the resonance position R=1.792 m, this gyrotron is expected to give enough current drive with 0.7 MW power; since the density was not high, no cutoff was detected.

Two NBI systems, NBI1 and NBI2, are used to compare the deposition profiles of 4 neutral beam sources in this experiment. All of the three beam sources in NBI1 are used in plasma core heating and approaching H-mode, as it has been successfully utilized as a main external heating source with 5.5 MW from 3 beam sources for the last decade. For the second NBI system, only NBI2-B is used since the other beam sources are not operational yet. NBI2 is designed to provide on-axis and off-axis current drive by arranging the three beam sources vertically. NBI2-A is an on-axis beam as NBI1, while NBI2-B and NBI2-C are up-looking and down-looking beams, respectively. The configuration of the two NBI systems is shown in Fig. 2. NBI2-B is more favorable to pitch angle alignment, so its operation started first.

In this experiment, NBCDs of NBI1 and NBI2-B are explored by switching off a single beam source for 1 s, which is longer than the current diffusion time scale, in a fully non-inductive discharge. The loop voltage remains close to zero during the shot. The plasma current is decomposed to NBCD, ECCD, and bootstrap current by NUBEAM [12–14] analysis with this condition, $I_p \sim I_{NI} = I_{NBCD} + I_{ECCD} + I_{BS}$.

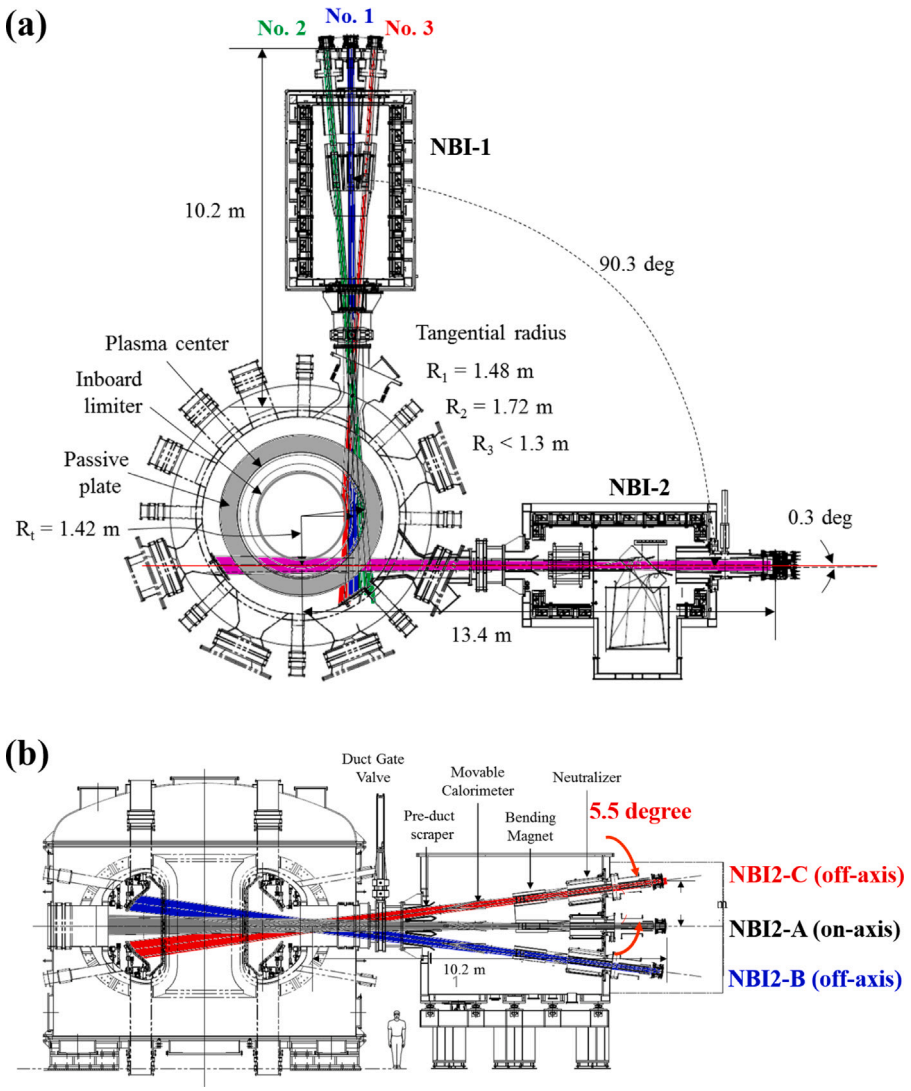

Fig. 2. (a) Arrangement of KSTAR NBI1 and NBI2 in top view. (b) A side view of KSTAR NBI2 [10].

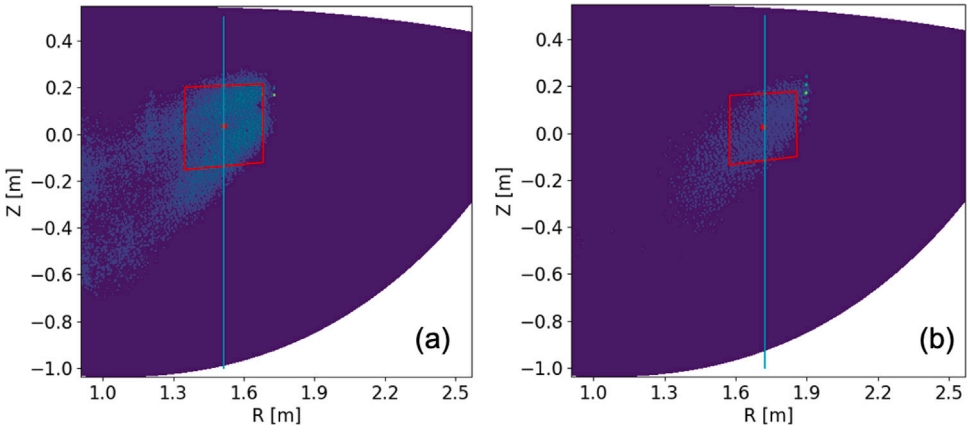

Fig. 3. CCD [11] Data obtained for the beam deposition of source NBI1-A(a) and NBI1-B(b).

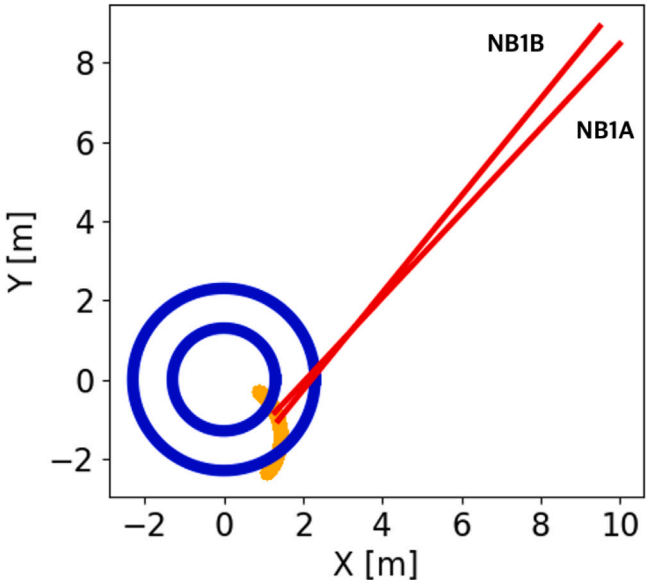

Fig. 4. Inferred beam injection geometry of NBI1-A and NBI1-B in a bird view of KSTAR geometry.

3. Neutral beam deposition profile

Experimental data processing and numerical modeling are conducted to derive NBI deposition profile. Two different methods were prepared and the results are compared with experimental and modeling values of NBI. One is beam footprint imaging to find beam injection location in Section 3.1 and the other one is an estimation of beam component from the total reconstructed current profile in Section 3.2

3.1. Evaluation of the position of the neutral beam injection

To clarify beam path modeling, the beam footprint is pictured with the fast camera system [11]. Accelerated and neutralized fast particle paths are confirmed. Considering the camera installation location, evaluation of the tangential position of the neutral beam is conducted at the poloidal cross section. A simple data processing script is utilized in order to analyze camera data. The algorithm of this program consists of the following steps: (1) Gather and add up the data for a given time-frame (2) Generate an analysis window (defined by height, width and position) and return the sum of all the data contained in this analysis window. (3) Move the analysis window over the whole analysis domain, in order to find the position of the maximum value returned by step 2. It is assumed that this position corresponds to the position of the beam center, observed on the camera. (4) Use the NBI source location and the position obtained in step 3, to determine the tangential position of the neutral beam injection.

Here, the results are obtained with the data from specific KSTAR discharge, which is designed to measure beam deposition. This shot consists of sequential injection of single beam source one by one into a high-density deuterium gas. Pressure at the main chamber is about 10^{-3} mbar. There is no external magnetic field from toroidal and poloidal field coils.

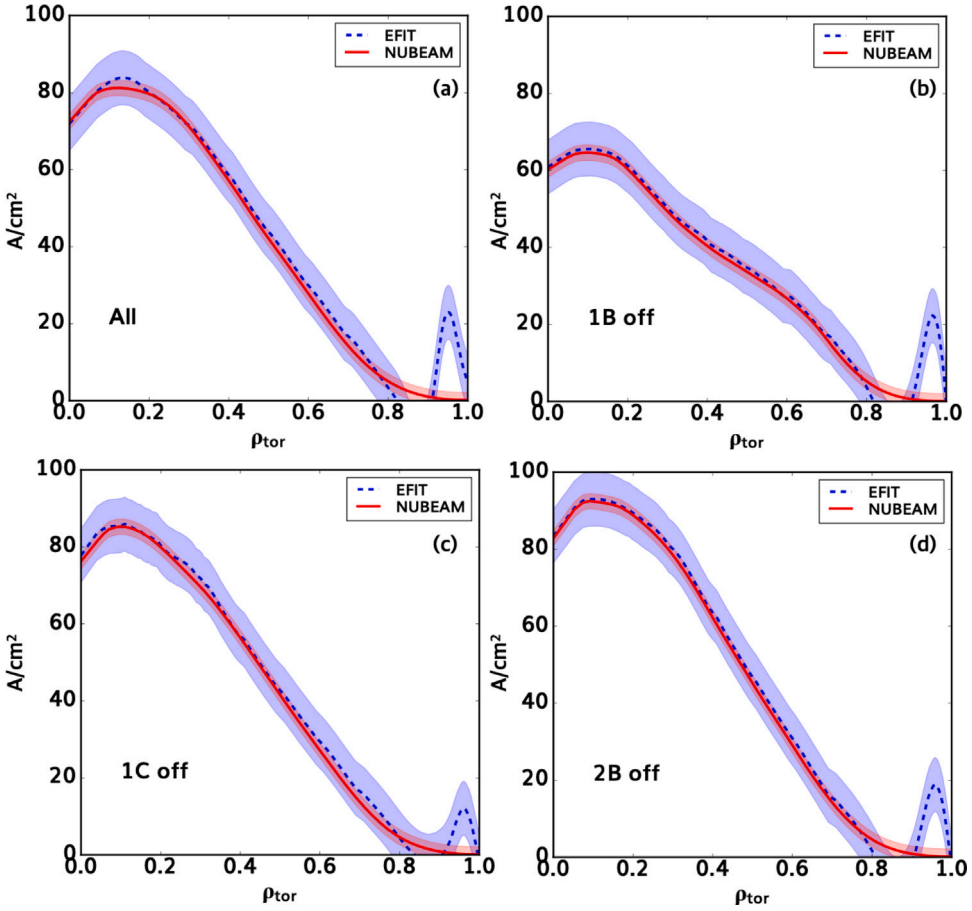

Fig. 5. Comparison neutral beam current drive profile from EFIT and NUBEAM. Since each neutral beam is turned-off one by one, regarding four time slices in Fig. 1 are selected: (a) 5.95 s with all beam (b) 6.8 s with NBI1-B off (c) 7.85 s with NBI1-C off (d) 8.85 s with NBI2-B off.

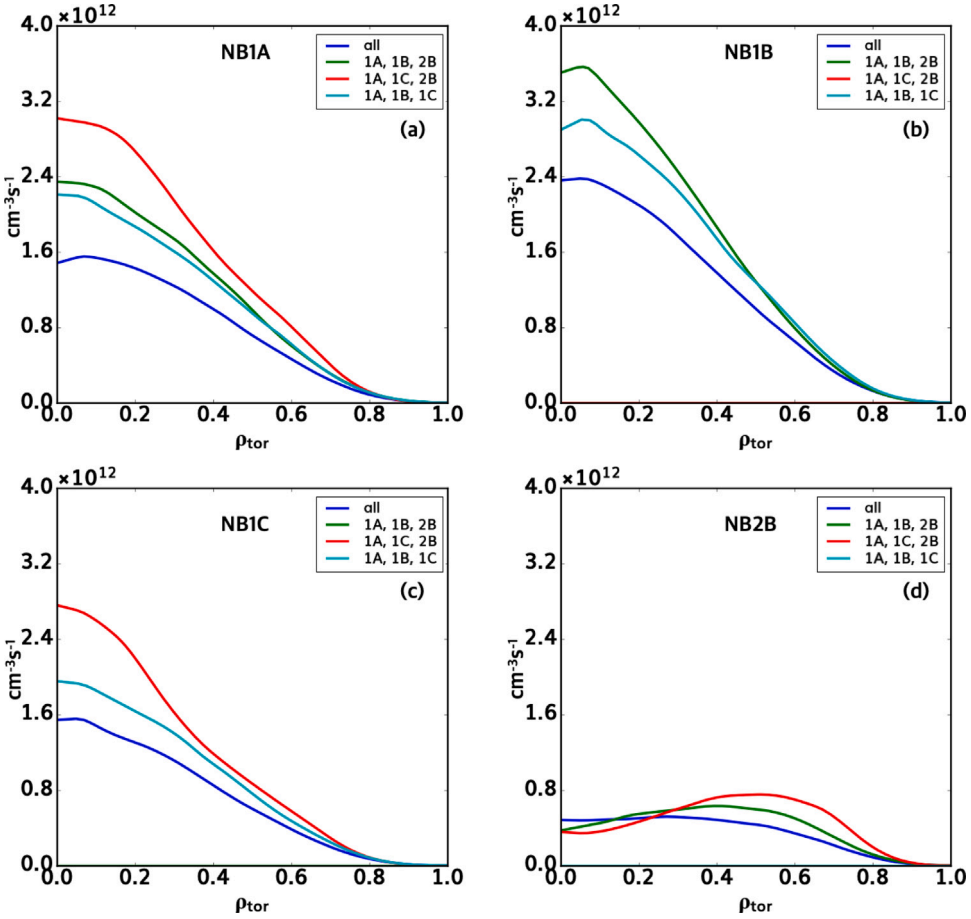

Fig. 6. Shot 27281 number beam deposition profiles of NBI1-A(a), NBI1-B(b), NBI1-C(c), and NBI2-B(d). At each figure time is from Fig. 5(a,b,c,d).

Fig. 3 shows the poloidal location and Fig. 4 visualizes the radial position obtained for sources NBI1-A and NBI1-B, respectively. The red square corresponds to the analysis window that contains the maximum injection. The red point corresponds to the center of this window. In the NBI1-A case as shown in Fig. 3(a), the radial position on the picture is 1514 mm, corresponding to a tangential position of 1486 mm. In the NBI1-B case, the radial position is 1717 mm, which corresponds to a tangential position of 1692 mm. The vertical blue line in Fig. 3 corresponds to the expected radial position of the beam, obtained from the KSTAR NBI geometry design. For those two sources, measured points and designed targets are quite consistent. However, it must be noted that there is no good result for sources NBI1-C and NBI2-B. Concerning source NBI1-C, the NB trajectory is inward, and the data observed are disturbed by the NBI shine-through. For the source NBI2-B, the NBI trajectory does not intersect the camera; so, there is no observable data. Therefore, those two beam paths are assumed that it is separated from NB1-A and NB1-B as much as the blueprint. Fig. 4 shows the results of the beam deposition analysis. The blue circles correspond to the inner and outer plasma boundary limits. The orange curved line shows the pixel position of the camera. The red lines show the NBI trajectory from the source to the image captured by the camera. Finally, this information is then used to determine the tangential position of the neutral beam deposition and transferred to input data for the next subsection analysis.

3.2. Reconstruction of neutral beam deposition profile

Since beam deposition profile cannot be directly measured in KSTAR in current diagnostic system, an alternative strategy is applied to infer beam deposition profile. First of all, beam driven current profile from equilibrium reconstruction ($J_{NB,EFIT}$) and beam driven current profile from modeling ($J_{NB,NUBEAM}$) are compared to verify the accuracy of NUBEAM. The MHD equilibrium and its total current profile are reconstructed from kinetic EFIT [15] with MSE [16] and kinetic constraints. Subtracting computed external current profile from TRANSP [17] from the reconstructed total current profile ,($J_{NB,EFIT}$) is estimated. ($J_{NB,EFIT} = J_{TOTAL,EFIT} - J_{bootstrap,TRANSP} - J_{ECCD,TRANSP} - J_{Ohmic,TRANSP}$) Fig. 5 shows comparison results of $J_{NB,EFIT}$ and $J_{NB,NUBEAM}$. Beam injection location used in NUBEAM analysis is from Section 3.1. Except edge region ($\rho_{tor} > 0.8$), all regions show consistent profile between reconstructed one and computed one. The edge regime has relatively more error-source, such as diagnostic and bootstrap current estimation.

Finally, the beam deposition profile could be inferred with NUBEAM modeling based on the validation processes above. Beam shield current is computed neoclassical way [18] and Z effective profile is assumed to be constant value 2. NUBEAM beam ion confinement coefficient is adjusted to match total neutron rate and total stored energy. Fig. 6 is the result of beam deposition profile from NUBEAM. At each figure, there are four different time slices where one of the beam source

is off, and they have their particular plasma characteristics such as collisionality and beam ion slowing-down time. Therefore, the amount of beam deposition could be different with the same injection power, but the peaking position is consistent among the four used sources. The NBI1 system targets to plasma core and the second beam system aims at the off-axis region. This inferred beam deposition profile result suggests that the neutral beam aiming target position is well-aligned with the original design. Finally, it confirms that NB system commissioning has been successfully finished for NB1-A, NB1-B, NB1-C, and NB2-B.

4. Conclusion

KSTAR has been operated more than a decade with neutral beam systems. The diagnostics system and the numerical modeling capabilities have matured enough to enable the integrated interpretation. The neutral beam deposition profile is a critical ingredient for almost every physics interpretation in KSTAR and the integrated analysis is essential to show its profile. In this paper, the dedicated experiment has been conducted to investigate deposition profiles. The reconstructed NBCD profile and computed one shows consistent results. Finally, the neutral beam deposition profile has been successfully evaluated and supports the successful commissioning process of neutral beam system.

CRediT authorship contribution statement

B. Na: Conceptualization, Investigation, Writing. **J. Kang:** Conceptualization, Methodology, Formal analysis, Investigation, Writing. **M.W. Lee:** Methodology, Formal analysis, Data curation. **L. Jung:** Methodology, Formal analysis, Writing. **S.H. Hahn:** Conceptualization, Methodology, Investigation, Writing. **J.W. Yoo:** Investigation, Methodology. **J.H. Jeong:** Investigation, Methodology. **J. Ko:** Formal analysis, Investigation, Validation. **C. Sung:** Methodology, Formal analysis, Data curation.

Declaration of competing interest

The authors declare that they have no known competing financial interests or personal relationships that could have appeared to influence the work reported in this paper.

Data availability

Data will be made available on request.

Acknowledgments

This research was supported by R&D Program of "KSTAR Experimental Colaboration and Fusion Plasma Research (EN-2201)" and "Development of ITER Heating and Current Drive Technology (IN2205)" through the Korea Institute of Fusion Energy(KFE) funded by the government funds, Republic of Korea. Part of the data analysis was performed using the OMFIT integrated modeling framework. [19] Authors deeply appreciate big supports from TRANSP team and providing TRANSPgrid server for computation.

References

[1] G. Lee, M. Kwon, C. Doh, B. Hong, K. Kim, M. Cho, W. Namkung, C. Chang, Y. Kim, J. Kim, H Jhang, D. Lee, K. You, J. Han, M. Kyum, J. Choi, J. Hong, W. Kim, B. Kim, J. Choi, S. Seo, H. Na, H Lee, S. Lee, S. Yoo, B. Lee, Y. Jung, J. Bak, H. Yang, S. Cho, K. Im, N. Hur, I. Yoo, J. Sa, K. Hong, G. Kim, B. Yoo, H. Ri, Y. Oh, Y. Kim, C. Choi, D. Kim, Y. Park, K. Cho, T. Ha, S. Hwang, Y. Kim, S. Baang, S. Lee, H. Chang, W. Choe, S. Jeong, S. Oh, H. Lee, B. Oh, B. Choi, C. Hwang, S. In, S. Jeong, I. Ko, Y. Bae, H. Kang, J. Kim, H. Ahn, D. Kim, C. Choi, J. Lee, Y. Lee, Y. Hwang, S. Hong, K.H. Chung, D.I. Choi, K. Team, Nucl. Fusion 41 (2001) 1515–1523, http://dx.doi.org/10.1088/0029-5515/41/10/318.

[2] T.S. Kim, S.H. Jeong, D.H. Chang, K.W. Lee, S.R. In, Rev. Sci. Instrum. 85 (2014) 02B311, http://dx.doi.org/10.1063/1.4827682.

[3] K. Kim, H. Park, H. Kim, K. Lee, N. Song, S. Kwag, Y. Chang, W. Cho, J. Kim, J. Jeong, K. Park, Y. Kim, Fusion Eng. Des. (ISSN: 0920-3796) 146 (2019) 1786–1789, sI:SOFT-30, URL https://www.sciencedirect.com/science/article/pii/S0920379619303576.

[4] J. Jeong, H. Ahn, W. Cho, Y. Kim, Fusion Eng. Des. (ISSN: 0920-3796) 169 (2021) 112479, URL https://www.sciencedirect.com/science/article/pii/S0920379621002556.

[5] T. Suzuki, R. Akers, D. Gates, S. Günter, W. Heidbrink, J. Hobirk, T. Luce, M. Murakami, J. Park, M T, Nucl. Fusion 51 (2011) 083020, http://dx.doi.org/10.1088/0029-5515/51/8/083020.

[6] S. Gerhardt, E. Fredrickson, D. Gates, S. Kaye, J. Menard, M. Bell, R. Bell, B.L. Blanc, H. Kugel, S. Sabbagh, H. Yuh, Nucl. Fusion 51 (2011) 033004, http://dx.doi.org/10.1088/0029-5515/51/3/033004.

[7] J.M. Park, M. Murakami, C.C. Petty, W.W. Heidbrink, T.H. Osborne, C.T. Holcomb, M.A. Van Zeeland, R. Prater, T.C. Luce, M.R. Wade, M.E. Austin, N.H. Brooks, R.V. Budny, C.D. Challis, J.C. DeBoo, J.S. deGrassie, J.R. Ferron, P. Gohil, J. Hobirk, E.M. Hollmann, R.M. Hong, A.W. Hyatt, J. Lohr, M.J. Lanctot, M.A. Makowski, D.C. McCune, P.A. Politzer, H.E. St John, T. Suzuki, W.P. West, E.A. Unterberg, J.H. Yu, Phys. Plasmas 16 (2009) 092508, http://dx.doi.org/10.1063/1.3213614, Preprint.

[8] B. Grierson, M.V. Zeeland, J. Scoville, B. Crowley, I. Bykov, J. Park, W. Heidbrink, A. Nagy, S. Haskey, D. Liu, Nuclear Fusion 61 (2021) 116049, http://dx.doi.org/10.1088/1741-4326/ac2872.

[9] Y.M. Jeon, et al., Distinctive feature of kstar stationary high poloidal beta scenario, in: 16th IAEA H-Mode Workshop, 2017.

[10] Y.K. Oh, S. Yoon, Y.m. Jeon, W.h. Ko, S.H. Hong, H.H. Lee, J.M. Kwon, M. Choi, B.H. Park, J.G. Kwak, W.C. Kim, Y.U. Nam, S. Wang, J.H. Jeong, K.R. Park, Y.s. Kim, Y. In, H.K. Park, G. Yun, W. Choe, Y.C. Ghim, Y.s. Na, Y.S. Hwang, J. Korean Phys. Soc. 73 (2018) 712–735, URL http://link.springer.com/10.3938/jkps.73.712.

[11] J. Yoo, J. Kim, M. Kim, S. Park, B. Park, Y. Nam, J. Kim, H. Wi, M Lehnen, W Kim, Fusion Eng. Des. (ISSN: 0920-3796) 174 (2022) 112984, URL https://www.sciencedirect.com/science/article/pii/S0920379621007596.

[12] R.J. Hawryluk, et al., An Empirical Approach to Tokamak Transport Physics of Plasmas Close to Thermonuclear Conditions, CEC, Brussels, 1980.

[13] R. Goldston, D. McCune, H. Towner, S. Davis, R. Hawryluk, G. Schmidt, J. Comput. Phys. (ISSN: 0021-9991) 43 (1981) 61–78, URL https://www.sciencedirect.com/science/article/pii/002199918190111X.

[14] A. Pankin, D. McCune, R. Andre, G Bateman, A. Kritz, Comput. Phys. Commun. (ISSN: 0010-4655) 159 (2004) 157–184, URL https://www.sciencedirect.com/science/article/pii/S0010465504001109.

[15] L. Lao, J. Ferron, R. Groebner, W. Howl, H.S. John, E. Strait, T. Taylor, Nucl. Fusion 30 (1990) 1035–1049, http://dx.doi.org/10.1088/0029-5515/30/6/006.

[16] J. Ko, J. Chung, Rev. Sci. Instrum. 88 (2017) 063505, http://dx.doi.org/10.1063/1.4986461.

[17] J. Breslau, M. Gorelenkova, F. Poli, J. Sachdev, A. Pankin, G. Perumpilly, X. Yuan, L. Glant, U.O. of Science, Transp (2018) URL https://www.osti.gov/biblio/1489900.

[18] S.P. Hirshman, Phys. Fluids 21 (1978) 1295–1301, (Preprint). https://aip.scitation.org/doi/pdf/10.1063/1.862397, URL https://aip.scitation.org/doi/abs/10.1063/1.862397.

[19] O. Meneghini, S. Smith, L. Lao, O. Izacard, Q. Ren, J. Park, J. Candy, Z. Wang, C. Luna, V. Izzo, B. Grierson, P. Snyder, C. Holland, J. Penna, G. Lu, P. Raum, A. McCubbin, D. Orlov, E. Belli, N. Ferraro, R. Prater, T. Osborne, A. Turnbull, G. Staebler, Nucl. Fusion 55 (2015) 083008, URL http://iopscience.iop.org/article/10.1088/0029-5515/55/8/083008/meta.